Iso-geometric Finite Element Analysis
Based on Catmull-Clark Subdivision Solids

D. Burkhart[†] and B. Hamann[‡] and G. Umlauf[§]

Abstract

We present a volumetric iso-geometric finite element analysis based on Catmull-Clark solids. This concept allows one to use the same representation for the modeling, the physical simulation, and the visualization, which optimizes the design process and narrows the gap between CAD and CAE. In our method the boundary of the solid model is a Catmull-Clark surface with optional corners and creases to support the modeling phase. The crucial point in the simulation phase is the need to perform efficient integration for the elements. We propose a method similar to the standard subdivision surface evaluation technique, such that numerical quadrature can be used.

Experiments show that our approach converges faster than methods based on tri-linear and tri-quadratic elements. However, the topological structure of Catmull-Clark elements is as simple as the structure of linear elements. Furthermore, the Catmull-Clark elements we use are C^2-continuous on the boundary and in the interior except for irregular vertices and edges.

Categories and Subject Descriptors (according to ACM CCS):

1. Introduction

Finite element methods are used in various areas ranging from mechanical engineering [Mer09] to computer graphics [ISF07] and bio-medical applications [BN96]. In engineering, one of the major problems is still the gap between computer-aided design (CAD) and computer-aided engineering (CAE). This gap results from different tools for the design based on exact geometries, like boundary representations or NURBS, and for the simulation based on approximative mesh representations.

The process of converting exact geometries to meshes is time-consuming and causes approximation errors. Although, in some instances meshes can be created automatically, often mesh creation is the most time consuming part. For automotive, aerospace, and ship industry it is estimated that the mesh creation consumes about 80% of the overall computational design process [BCC*10]. As design and analysis are typically done in sequence and sometimes even in multiple design iteration loops, it is necessary to convert data between CAD and CAE systems repeatedly. Thus, a change of the

CAD geometry requires an adaptation of the CAE geometry before the simulation can be repeated.

We present a method using Catmull-Clark solids for the geometric modeling and the physical simulation, to narrow the gap between CAD and CAE. We refer to the elements of the solids as Catmull-Clark elements. We restrict the solid topology to three-manifold meshes of hexahedra with arbitrary edge and vertex connectivity.

Our method is illustrated in Figure 2. In the initial phases the boundary surface is modeled, the interior of the model is meshed with hexahedra and the boundary conditions, such as external forces, are defined. These three steps are regarded as pre-processing and are not discussed in this paper. The boundary and the interior of the solid model are Catmull-Clark surfaces and Catmull-Clark solids, respectively, with optional sharp features such as corners and creases. Thus, the solid model is C^1-continuous away from the sharp feature in the limit. Subsequently, the solid model can be subdivided to increase the accuracy of the simulation. These rules are simpler than those for NURBS, especially for models with arbitrary topology. Next, the stiffness matrices are assembled. One obtains a system of equations to be solved and additional post-processing computations. These last two steps are the post-processing to our method and are not discussed in this paper. If the simulation results are inadequate

---

† University of Kaiserslautern, Germany, burkhart@cs.uni-kl.de
‡ University of California, Davis, USA, hamann@cs.ucdavis.edu
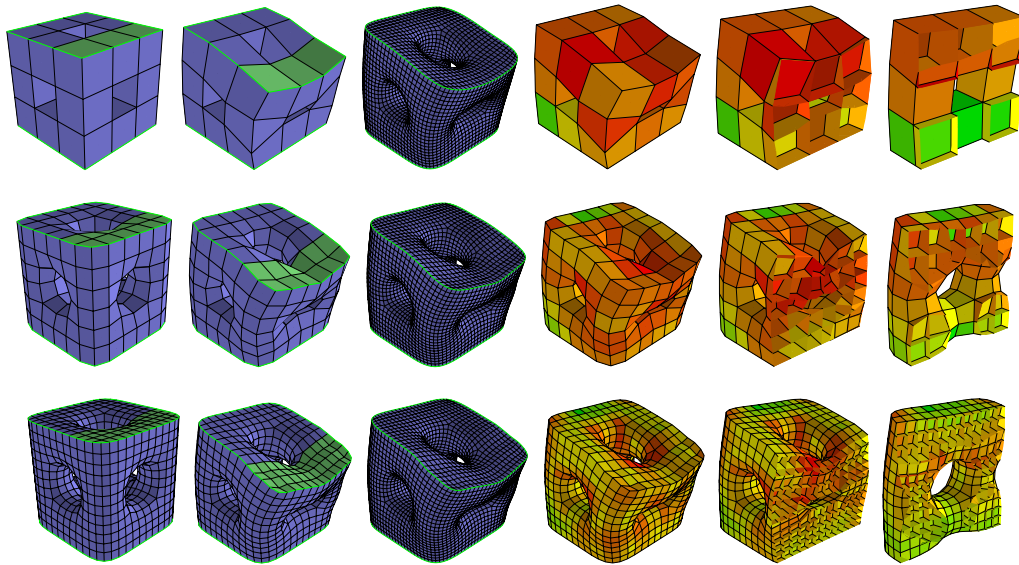§ HTWG Constance, Germany, umlauf@htwg-konstanz.de

Figure 1: *Deformation of a hexahedral mesh on three levels of refinement. First row: base mesh, second row: one-time refined mesh, third row: two-times refined mesh. First column: undeformed mesh, second column: deformed mesh, third column: deformed mesh after four steps of refinement, fourth column: deformation stress, fifth and sixth columns: cut-away view with stress in the interior. Green faces and green edges in columns one to three are loaded faces and feature edges, respectively. In columns four to six, the stress is visualized by the linearly interpolated color hue from $0°$ (high stress) to $120°$ (low stress).*

the geometric model can be adapted after the simulation and the whole process is repeated. As the same representation is used for the modeling and the simulation, these adaptations do not require data conversion.
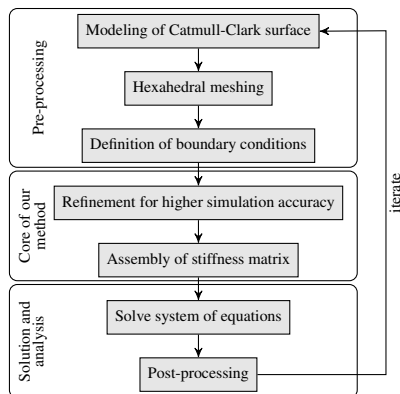

Figure 2: *Steps of our modeling and simulation framework.*

We demonstrate the efficiency and effectiveness of our approach for problems in structural mechanics. The basic concept is also applicable to problems in fluid dynamics, heat conduction or electromechanics. Figure 1 illustrates our approach for a simple input mesh. A vertical load is applied to the green faces, while the model is fixed at the bottom. The

problem is simulated on three levels of refinement. In Section 2 we discuss recent work on iso-geometric analysis and subdivision schemes. We briefly review subdivision surfaces and solids in Section 3. Standard finite element techniques for linear elasticity problems are described in Section 5. In Sections 6 and 7 we describe our approach for finite element analysis based on Catmull-Clark solids and demonstrate its effectiveness in Section 8.

2. Related Work

2.1. Iso-geometric analysis

The concept of iso-geometric analysis was originally proposed in [HCB05]. Here, the idea is to use the same geometric representation based on NURBS for the modeling and the simulation. Other representations like B-splines [KFBY99] or T-splines [BCC*10] were also used. Since the same model is used in both phases, there is no need to convert the NURBS to a mesh. As far as the simulation is concerned, an important aspect of these approaches is the fact that refinement or degree elevation can be used to increase the simulation accuracy without changing the geometry. The drawback of this approach is that the underlying grid must be a structured grid and that solid meshes are not supported.

In the pioneering works [COS00, CSA*02] a similar approach based on Loop-subdivision surfaces for the geometric modeling and the mechanical simulation of thin flexible

structures is proposed. The subdivision surfaces are used to describe both, the undeformed geometry and the smooth interpolated displacement field with Kirchhoff-Love theory of thin shells. Due to the usage of subdivision surfaces, this approach supports only unstructured two-manifold meshes.

2.2. Subdivision surfaces

Subdivision surfaces are a a standard modeling tool in computer graphics to model free-form surfaces [DKT98]. They were first developed in 1978 [CC78, DS78]. A subdivision surface is defined as the limit of an iterative refinement process, starting with a polygonal base mesh M_0 of control points. Iterating the subdivision process generates a sequence of refined meshes $M_1, \ldots, M_n$, that converges to a smooth limit surface M_∞ for $n \to \infty$. Usually the subdivision operator can be factored into a topological refinement operation followed by a geometrical smoothing operation. While the topological refinement inserts new vertices or flips edges, the geometrical smoothing changes vertex positions.

Subdivision surfaces either approximate or interpolate the base mesh. For approximating schemes the control points of M_i usually do not lie on M_{i+1}, $i \geq 0$. Approximating schemes for arbitrary quadrangle meshes are Doo-Sabin and Catmull-Clark subdivision [CC78, DS78]. Both are generalizations of uniform tensor-product B-spline surfaces. Approximating schemes for arbitrary triangle meshes the algorithm of Loop and $\sqrt{3}$-subdivision [Loo87, Kob00]. For interpolating schemes all control points of M_i are also in M_{i+1}, $i \geq 0$. Thus, the limit surface interpolates these points. An interpolating subdivision scheme for surfaces is the butterfly scheme of [DLG90].

While subdivision surfaces have continuous normals, real-world models have sharp features with discontinuous normals. To model these features subdivision algorithms are tailored to allow for corners and creases. Examples for such special rules, where tagged edges will yield creases on the subdivision surface, are presented in [BLZ00, BMZB02]. For more details on subdivision surfaces we refer to [PR08].

2.3. Subdivision solids

In contrast to subdivision surfaces, subdivision solids have gained much less attention. One of the first algorithms is described in [JM96, MJ96]. It is a generalization of Catmull-Clark subdivision to 3D solids for smooth deformations based on unstructured hexahedral meshes. As the topological refinement operation of this algorithm made it hard to analyze the smoothness of the resulting limit solid, a modified operation was proposed in [BSWX02]. The resulting deformations are provably smooth everywhere except at the vertices of the base mesh.

A subdivision scheme for tetrahedral meshes based on trivariate box splines was proposed in [CMQ02, CMQ03].

The topological refinement first splits every tetrahedron into four tetrahedra and one octahedron. Subsequently, every octahedron is split along one of its diagonals into six tetrahedra causing a potential directional bias. To remedy this effect Schaefer et al. [SHW04] use a topological refinement that splits the octahedra symmetrically into eight tetrahedra and six octahedra. Their geometric smoothing allows for globally C^2-continuous deformations, except along edges of M_0. The major drawback of these schemes is the use of tetrahedra and octahedra, which are not well-suited for finite volume simulations, and require a complicated data structure.

A solid subdivision scheme that supports arbitrary polyhedral elements and adaptive refinement was presented in [Pas02]. However, its topological refinement splits the polyhedra into pyramids causing complex merging operations in every subdivision step.

3. Subdivision

3.1. Catmull-Clark surfaces

The subdivision rules for Catmull-Clark surfaces are defined by the following four steps at a vertex of valence n:

1. For each face add a face point to its centroid.
2. For each edge add an edge point $E = (F_0 + 2M + F_1)/4$, where F_0 and F_1 are the face points of the two incident faces and M is the edge midpoint.
3. For each face connect its face point into all edge points. For quadrilaterals this operation splits each old quadrilateral to four new quadrilaterals.
4. Move each original vertex V_{old} to its new location $V_{new} = (F_{avg} + 2M_{avg} + (n-3)V_{old})/n$, where M_{avg} and F_{avg} are the averages of all adjacent edge and face points.

For boundaries and sharp features special rules are given in [BLZ00]. An example of the overall subdivision is shown in the top row of Figure 3.

All steps of Catmull-Clark subdivision are linear combinations. Thus, there is a linear operator that relates the mesh M_i to the finer mesh M_{i+1}, $i \geq 1$. This operator generates only regular vertices, i.e., vertices with valence four, and coincides in mesh regions with regular vertices only with uniform bi-cubic B-spline knot insertion. Therefore, this linear operator can be localized. There exists a so-called subdivision matrix S that relates each vertex and its two-ring neighborhood in M_i to the corresponding vertex in M_{i+1} and its refined two ring neighborhood. The subdivision matrix is usually parametrized by the valence n of the vertex.

4. Catmull-Clark solids

The solid subdivision scheme we use for the iso-geometric finite element analysis is the previously described Catmull-Clark scheme. The advantage of this scheme is its simplicity compared to the other subdivision solids. Starting with

a hexahedral base mesh, only hexahedral elements are generated, all new vertices are regular, i.e. they have six incident edges, and all new edges are regular, i.e. they have four incident hexahedra. However, this scheme can generate inverted hexahedra even from a non-self-intersecting hexahedral mesh. The subdivision rules for Catmull-Clark solids for hexahedral meshes are defined by five steps [JM96]:

1. For each hexahedron add a cell point to its centroid.
2. For each face add a face point $F = (C_0 + 2A + C_1)/4$, where C_0 and C_1 are the cell points of the two incident hexahedra and A is the face centroid.
3. For each edge add an edge point $E = (C_{avg} + 2A_{avg} + (n-3)M)/n$, where n is the number of incident faces, M is the edge midpoint, and C_{avg} and A_{avg} are the averages of cell and face points of incident cells and faces, respectively.
4. For each hexahedron connect its cell point to all its face points and connect all its face points to all incident edge points. This splits one hexahedron to eight hexahedra.
5. Move each original vertex V_{old} to its new location $V_{new} = (C_{avg} + 3A_{avg} + 3M_{avg} + V_{old})/8$, where C_{avg}, A_{avg}, and M_{avg} are the averages of the cell, face and edge points of all adjacent cells, faces, and edges.

For faces, edges and vertices on the boundary of the solid corresponding rules for Catmull-Clark surfaces are applied. An example of this algorithm is shown in Figure 3.

Also for Catmull-Clark solids there is a subdivision matrix that relates each vertex and its neighborhood in M_i to its corresponding vertex and neighborhood in M_{i+1} [BSWX02]. However, this matrix depends on the local mesh topology and is thus parametrized via a graph isomorphy.
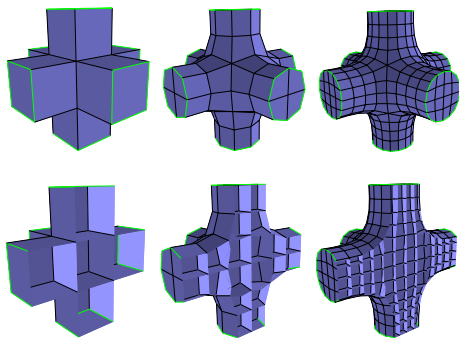

Figure 3: *Two steps of Catmull-Clark refinement applied to a hexahedral mesh with sharp boundary edges (green).*

5. Finite element analysis of elastic materials

Finite element analysis is a numerical method to solve partial differential equations by discretizing these equations in their spatial dimensions. This discretization is done locally in small regions of simple shape (the finite elements) connected at discrete nodes. The solution of the variational equations is

approximated with local shape functions defined for the finite elements. This results in matrix equations relating the input (boundary conditions) at the discrete nodes to the output at these nodes (the unknown variables). The contribution of each element is computed in terms of local stiffness matrices $\mathbf{K}_m$, which are assembled into a global stiffness matrix $\mathbf{K}$. This yields for static elasticity problems a linear system of equations $\mathbf{Ku} = \mathbf{f}$, where $\mathbf{u}$ is the vector of the unknown variables and $\mathbf{f}$ of the external forces. The computation of local stiffness matrices $\mathbf{K}_m$ depends on the physical problem and is described for linear elastic material in the sequel.
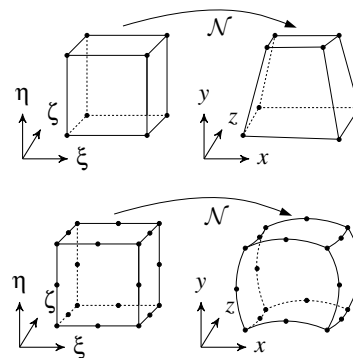

Figure 4: *Tri-linear (top) and tri-quadratic (bottom) Lagrangian hexahedral elements in local (left) and global coordinates (right) with respect to their shape functions $\mathcal{N}$.*

For volumetric problems the most common element types are hexahedra and tetrahedra. Typically, these elements are defined in a local coordinate system. This simplifies the construction of shape functions also for higher-order elements with curved boundaries and the numerical quadrature arising during the assembly of the stiffness matrix. If the same shape functions are used to describe the variation of the unknowns, such as displacement or fluid potential, and the mapping between the global and local coordinates, the elements are called iso-parametric elements.

A tri-linear and a tri-quadratic hexahedral element are illustrated in Figure 4, where (ξ, η, ζ) are local and (x, y, z) are global coordinates. The tri-linear element, for instance, has eight local shape functions $\mathcal{N} = [\mathcal{N}_1, ..., \mathcal{N}_8]$ defined over the cube $[-1, +1]^3$. For more details on elements of different order and their shape functions we refer to [SG04].

During the assembly of the stiffness matrix the shape functions and their derivatives with respect to global coordinates are involved. The conversion of these derivatives between the coordinate systems is provides by the Jacobian matrix. For the integration over the volume of the elements usually numerical integration such as Gauss-Legendre quadrature is used [PTVF07]. In one dimension

these quadrature rules are of the form

$$\int_{-1}^{+1} f(x)dx \approx \sum_{i=1}^{k} w_i \mathbf{f}(x_i),$$

where k is the number of integration points, w_i are the weights, and x_i are the sampling points. For $k = 2$ Gauss-Legendre quadrature is exact for cubic polynomials. The values for $k = 1, 2, 3$ are shown in Table 1.

k	x_i			w_i		
1		0			2	
2	$-\sqrt{1/3}$		$+\sqrt{1/3}$	1		1
3	$-\sqrt{3/5}$	0	$+\sqrt{3/5}$	5/9	8/9	5/9

Table 1: *Sampling points x_i and weights w_i for Gauss-Legendre quadrature of order $k = 1, 2, 3$.*

In the theory of linear elasticity, a solid model Ω consists of a set of nodes $\mathbf{x} = [x, y, z]^T$. These nodes are connected to form the elements for the finite element analysis. When forces are applied, Ω is deformed into a new shape. Thus, $\mathbf{x}$ is displaced to $\mathbf{x} + \mathbf{u}$ with $\mathbf{u}(\mathbf{x}) = [u, v, w]^T$. The boundary of the domain Ω consists of the boundary Γ_1 with fixed displacements $\mathbf{u}(\mathbf{x}) = \mathbf{u}_0(\mathbf{x})$, the boundary Γ_2 where forces are applied, and the boundary Γ_3 without constraints. These components satisfy $\Gamma = \bigcup_i \Gamma_i$ and $\bigcap_i \Gamma_i = \emptyset$.

The strain energy of a linear elastic body Ω is defined as

$$E_{strain} = \frac{1}{2} \int_{\Omega} \varepsilon^T \sigma \, d\mathbf{x},$$

with the stress vector σ and the strain vector $\varepsilon = [\varepsilon_x \ \varepsilon_y \ \varepsilon_z \ \gamma_{xy} \ \gamma_{xz} \ \gamma_{yz}]^T$ defined as

$$\varepsilon_x = \frac{\partial u}{\partial x}, \qquad \varepsilon_y = \frac{\partial u}{\partial y}, \qquad \varepsilon_z = \frac{\partial u}{\partial z},$$

$$\gamma_{xy} = \frac{\partial u}{\partial y} + \frac{\partial v}{\partial x}, \quad \gamma_{xz} = \frac{\partial u}{\partial z} + \frac{\partial w}{\partial x}, \quad \gamma_{yz} = \frac{\partial v}{\partial z} + \frac{\partial w}{\partial y}.$$

This can be rewritten as $\varepsilon = \mathbf{B}u$, where $\mathbf{B}$ is the so-called strain-displacement matrix, that depends on the partial derivatives of the shape functions of used finite elements

$$\mathbf{B}^T = \begin{bmatrix} \partial/\partial x & 0 & 0 & \partial/\partial y & \partial/\partial z & 0 \\ 0 & \partial/\partial y & 0 & \partial/\partial x & 0 & \partial/\partial z \\ 0 & 0 & \partial/\partial z & 0 & \partial/\partial x & \partial/\partial y \end{bmatrix}. \quad (1)$$

Hooke's law $\sigma = \mathbf{C}\varepsilon$ relates the stress vector σ to ε via the material matrix $\mathbf{C}$, which is defined by the Lamé constants λ and μ. Rewriting the strain energy and adding work applied by internal and external forces $\mathbf{f}$ and $\mathbf{g}$, respectively, yields the total energy function

$$E(\mathbf{u}) = \frac{1}{2} \int_{\Omega} \mathbf{u}^T \mathbf{B}^T \mathbf{C} \mathbf{B} \mathbf{u} \, d\mathbf{x} - \int_{\Omega} \mathbf{f}^T \mathbf{u} \, d\mathbf{x} - \int_{\Gamma_2} \mathbf{g}^T \, d\mathbf{a}. \quad (2)$$

A detailed discussion is provided in [ZT00, SG04].

6. Assembly of Catmull-Clark solids

We use Catmull-Clark solids for the representation of the geometry and the approximation of the displacement field defined by Equation (2). To solve this equation the finite element method is used to define a linear system of equations of the form $\mathbf{K}\mathbf{u} = \mathbf{f}$, where $\mathbf{K}$ is the global stiffness matrix, $\mathbf{u}$ is the unknown displacement vector and $\mathbf{f}$ are the external forces. The global stiffness matrix $\mathbf{K}$ is defined via the element stiffness matrices

$$\mathbf{K}_m = \int \int \int \mathbf{B}^T \mathbf{C} \mathbf{B} \, dx dy dz. \quad (3)$$

As the exact evaluation of (3) is in general not possible, three-dimensional Gauss-Legendre quadrature is used:

$$\int_{-1}^{+1} \int_{-1}^{+1} \int_{-1}^{+1} \mathbf{f}(x, y, z) dx dy dz \approx \sum_{i=1}^{n} W_i \mathbf{f}(x_i, y_i, z_i), \quad (4)$$

where x_i, y_i and z_i are permutations of the sampling points of the univariate quadrature rule and W_i is the product of the corresponding weights. As the elements are defined in local coordinates, (4) in combination with (3) yields

$$\mathbf{K}_m \approx \sum_{i=1}^{n} W_i \det(\mathbf{J}) \mathbf{B}^T \mathbf{C} \mathbf{B}. \quad (5)$$

The assembly is illustrated in Procedure 1, where line nine implements equation (5). In lines two and three the number of nodes m in the one ring of an element is used to initialize the element stiffness matrix $\mathbf{K}_m$. In line six the derivatives $\mathbf{D}$ of the basis functions for the Catmull-Clark elements at the current sampling point p are computed. This function will be discussed in Section 7.3 in detail. As these derivatives are computed in local coordinates ξ, η, ζ, the Jacobian $\mathbf{J}$ is computed from the global coordinates of the current hexahedron Coordinates(h) (line seven) for the conversion to global coordinates x, y, z. Using the Jacobian $\mathbf{J}$ and the derivatives $\mathbf{D}$, the strain-displacement matrix $\mathbf{B}$ computed in AssembleB($\mathbf{J}$, $\mathbf{D}$) according to (1). Every part of Procedure 1 can also be used for standard elements except the computation of the derivatives, that is tailored for Catmull-Clark solids.

For standard tri-linear and tri-quadratic elements these derivatives can be computed directly. For Catmull-Clark elements it is not obvious how to compute derivatives due to topologically arbitrary elements as shown in Figure 5(b). However, evaluations of topological arbitrary elements can be reduced to evaluations of regular elements shown in Figure 5(a). These regular elements can be evaluated directly, see Section 7.1. The evaluation for the irregular elements is discussed in Section 7.2. Thus, our approach can be integrated with the iso-parametric concept since the same program code can be used as the one used for the standard finite elements from Figure 4. Only the evaluation at the sampling points needs to be adapted to the arbitrary topological setting illustrated in Figure 5(b).

Once the stiffness matrix $\mathbf{K}$ is assembled, the force vector

Procedure 1 AssembleCCElements(HexMesh *m*)

1: **for all** (HexCC *h* in *m*) **do**
2:      *m*   = NumberOfNodesInOneRing(*h*);
3:      $\mathbf{K}_m$ = InitMatrix($3 \cdot m$, $3 \cdot m$);
4:      **for** (**int** $i = 0$; $i < n$; $i + +$) **do**
5:          *p*   = SamplePoint(*i*);
6:          $\mathbf{D}$ = Derivative(*h*, *p*);
7:          $\mathbf{J}$ = $\mathbf{D} \cdot$ Coordinates(*h*);
8:          $\mathbf{B}$ = AssembleB($\mathbf{J}$, $\mathbf{D}$);
9:          $\mathbf{K}_m += W_i \cdot \det(\mathbf{J}) \cdot \mathbf{B}^T \cdot \mathbf{C} \cdot \mathbf{B}$; // see (5)
10:     **end for**
11:     Assemble($\mathbf{K}$, $\mathbf{K}_m$);
12: **end for**

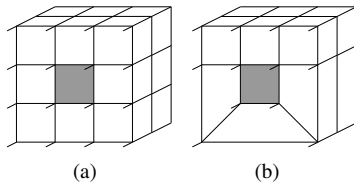

(a)   (b)

Figure 5: *Regular Catmull-Clark element (left), irregular Catmull-Clark element (right). To evaluate the highlighted hexahedron, all neighbored hexahedra are required.*

$\mathbf{f}$ can be constructed. Fixed displacements are enforced using the penalty method described in [SG04]. Finally, the linear system of equations $\mathbf{Ku} = \mathbf{f}$ can be solved with standard linear solvers. To derive the deformed geometry the computed displacement field is applied to the original geometry. The relation $\varepsilon = \mathbf{Bu}^e$ yields the strain at the sampling points of the Gauss-Legendre quadrature for each element, where $\mathbf{u}^e$ is the displacement vector for a single element. With Hooke's law $\sigma = \mathbf{C}\varepsilon$ the stress is computed.

7. Evaluation of Catmull-Clark solids

Using Catmull-Clark solids for finite element analysis, the displacement field within an element does not only depend on the displacements of the nodes attached to the element but also on the displacements of the nodes of adjacent elements, because the support of the basis functions of Catmull-Clark solids overlaps a one-ring neighborhood of elements. Hence, for the evaluation at the sampling points of the Gauss-Legendre quadrature, the one-ring neighborhood around an element is required. This is illustrated in Figure 5, where the gray elements are evaluated and all adjacent elements are required for the evaluation.

7.1. The regular case

As Catmull-Clark solids generalize tri-cubic uniform B-splines to arbitrary topology, cubic uniform B-spline basis functions can be used, provided the element has no

irregular vertex, see Figure 5(a). These regular elements depend on 64 nodal positions. The associated basis functions for $(s, t, u) \in [0, 1]^3$ and $i, j, k = 0, \dots, 3$ are given by $N_{ijk}(s, t, u) = N_i(s)N_j(t)N_k(u)$, where $N_0, \dots, N_3$ are the uniform cubic B-spline functions.

7.2. The irregular case

If a hexahedral element has at least one irregular vertex, as shown in Figure 5(b), this technique cannot be applied. However, a technique similar to [Sta98, Sta99] for the evaluation of subdivision surfaces at arbitrary parameter values can be used. This technique is based on the diagonalization of the subdivision matrix *S*, where the eigenvectors can be interpreted as instances of special regular meshes. These can be precomputed symbolically and evaluated with the B-spline evaluation as discussed in Section 7.1. Thus, iterating the subdivision process means scaling these special eigenvector meshes with powers of the corresponding eigenvalues. This reduces the evaluation at an arbitrary parameter value to the computation of the correct power of the eigenvalue and B-spline evaluations of the tabulated eigenvector meshes.

This technique is not immediately applicable to and required for our application. First, the eigenvectors of the subdivision matrix are parametrized by a graph isomorphy, which requires the symbolical pre-computation of a large number of eigenvectors. Second, for the quadrature rules the subdivision solids are only evaluated at the sample points.

To evaluate a Catmull-Clark solid at the eight sample points of Gauss-Legendre quadrature of order $k = 2$ using standard B-spline evaluation each sample point must lie in the central element of a regular $3 \times 3 \times 3$ mesh neighborhood. Because one subdivision step bisects the corresponding parameter space, after at most $\ell = 2$ subdivisions every sample point of M_i satisfies this requirement in $M_{i+\ell}$. For 27 and 64 sample points of Gauss-Legendre quadrature of order $k = 3, 4$, at most $\ell = 4$ subdivision steps are required. This is used to compute the 192 derivatives of the basis functions

$$\frac{d}{d\omega}N_{ijk}(s, t, u), \qquad i, j, k \in \{0, \dots, 3\}, \omega \in \{s, t, u\}.$$

Note that the derivatives are scaled by $2^{-\ell}$. Instead of the eigenvectors we pre-compute the evaluation rules.

7.3. Evaluation algorithm

The assembly of Catmull-Clark elements is more expensive than the assembly of eight-node hexahedral elements for two reasons. First, eight-node hexahedral elements have 24 degrees of freedom, while Catmull-Clark elements have in the regular case 192 degrees of freedom. This means that the matrix-matrix multiplications in Equation (3) are more expensive. This can only be handled by a suitable optimized matrix library. Second, the computation of the derivatives at the sampling points is more expensive. To optimize this,
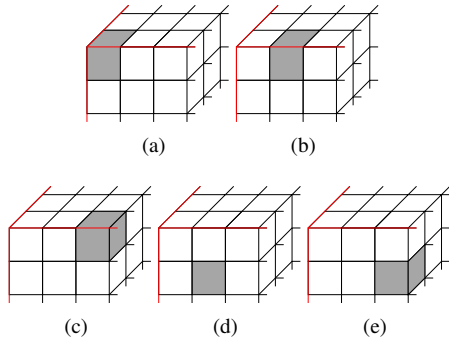
Figure 6: *Five isomorphy classes for a regular hexahedral mesh with feature edges in red.*

we pre-compute and buffer stencils for the derivatives at the sampling points. For all identical one-ring neighborhoods the computations have to be done only once.

For regular meshes there is only a small number of isomorphic one-ring neighborhoods. Five of these are shown in Figure 6. For arbitrary hexahedral meshes it is more complex to determine isomorphic one-ring neighborhoods, since this is an instance of a graph isomorphism problem [GJ90] which is NP-complete. Here the valence of an interior vertex does not suffice to determine the local mesh topology uniquely. To find isomorphic cases we construct weighted undirected graphs of the sub-meshes containing one hexahedron and its one-ring neighborhood. In the regular case this graph consists of 64 nodes and 288 edges. The weights of the edges of this graph correspond to the tags representing the features of the geometric model. For complicated meshes an additional hashing of the graphs avoids many unnecessary graph comparisons. The hash function we use is

$$h = 3n_e + 5n_v + 7n_h + \sum_{i=1}^{n_e} e_i, \qquad (6)$$

where e_i is the tag of the i-th edge and n_e, n_v, and n_h are the number of edges, vertices, and hexahedra in the sub-mesh.

Procedure 2 shows the function to evaluate derivatives of Catmull-Clark elements at a sampling point p schematically. Here, the matrices $\mathbf{D}$ and $\mathbf{S}$ represent the derivatives and the subdivision stencils. The size of $\mathbf{D}$ depends on the number of vertices in the one-ring neighborhood of the hexahedron, which is 3×192 in the regular case. The irregular mesh shown in Figure 5(b) has 48 vertices and $\mathbf{D}$ has size 3×144.

In line three the sub-mesh containing the hexahedron to be evaluated and its one-ring neighborhood are extracted. Then first the isomorphism class of this mesh configuration is checked (line five) using the hash function (6). If this mesh configuration is not yet been evaluated, i.e. is not in the database, the sub-mesh is subdivided (line eight) and the parameters u, v, w are adapted (lines nine to eleven) until the

sampling point lies in a regular sub-mesh. During each step of refinement the stencil $\mathbf{S}$ is adapted too. In line 13 and 14 the derivatives for a regular one-ring neighborhood for the current parameters u, v, w and for the original irregular sub-mesh are computed. The function of the stencil $\mathbf{S}$ is used to map the regular subdivided sub-mesh *temp* to the irregular original sub-mesh *sub*. Hence, the size of $\mathbf{S}$ depends on the number of vertices in *sub*, e.g. for the irregular mesh shown in Figure 5(b) $\mathbf{S}$ has the size 192×144. Finally, the stencil and derivative are stored in a database (line 15).

Procedure 2 Derivative(HexCC h, Point3D p)

1: $u = p.x$; $v = p.y$; $w = p.z$;
2: $level$=0;
3: sub = SubMesh(h);
4: $hash$ = CalcHash(sub);;
5: **if** ($\mathbf{D}$ = GetFromDataBase($hash$, sub)) **return D**;
6: **repeat**
7:    level++;
8:    temp = Subdivide(sub, $\mathbf{S}$);
9:    **if** ($u \leq 0.5$) $u = 2 \cdot u$; **else** $u = (u - 0.5) \cdot 2$;
10:   **if** ($v \leq 0.5$) $v = 2 \cdot v$; **else** $v = (v - 0.5) \cdot 2$;
11:   **if** ($w \leq 0.5$) $w = 2 \cdot w$; **else** $w = (w - 0.5) \cdot 2$;
12: **until** (IsRegular($temp$));
13: $\mathbf{D}$ = EvalBsplineDerivatives(u, v, w);
14: $\mathbf{D} = \mathbf{D} \cdot \mathbf{S} \cdot 2^{-level}$;
15: SaveToDataBase($hash$, sub, $\mathbf{D}$, $\mathbf{S}$);
16: **return D**;

---

8. Results

To demonstrate the effectiveness of our approach, we compare it to standard finite elements hex_8 and hex_{20} shown in Figure 4. As test case we use the model shown in Figure 7(a). This model is fixed at the left side and a vertical load is applied on the right side. We measure the maximum displacement in the direction of the load and compare this displacement. For the visualization of the displacement or stress fields we linearly interpolate the color hue from $0°$ (high displacement or stress) to $240°$ (low displacement or stress).

To show that our approach does not require a regular structured mesh, we use the unstructured mesh of this model shown in Figure 7(b). The model in Figure 7(a) consists of 221 hexahedra and 504 vertices. The hexahedra are equally sized cubes and vertices and edges are regular, except on boundaries. To generate the model shown in 7(b) we refined several hexahedra with an irregular split operation and moved the vertices randomly. This mesh consists of 800 hexahedra and $1,392$ vertices. The statistic of irregular vertices and edges in both meshes is shown in Table 2.

To analyze the convergence we subdivide both models twice and measure the rate of convergence with respect to a reference solution. The reference solution is the solution computed with hex_8 elements on the three times subdivided

Valence	Vertices in 7(a)	Edges in 7(a)	Vertices in 7(b)	Edges in 7(b)
1	0	250	0	196
2	0	652	0	1076
3	16	70	11	1616
4	172	222	826	381
5	244	0	256	61
6	72	0	104	43
7	0	0	79	21
8	0	0	53	14
≥9	0	0	63	6

Table 2: *Edge and vertex valence for the models shown in Figures 7(a) and 7(a).*

Figure 8: *Convergence analysis for the model shown in Figure 7(a) (continuous lines) and 7(b) (dashed lines).*

model shown in Figure 7(a), which consists of $113,152$ hexahedra, $129,059$ vertices and hence $387,177$ degrees of freedom. Due to the high number of degrees of freedoms, the reference solution was computed with a conjugate gradient solver. For all other meshes we assemble the stiffness matrices to sparse matrices and use the sparse direct solver SuperLU [DEG*99]. The line charts shown in Figure 8 illustrate the rate of convergence against the normalized error. The timings used in the chart include the assembly of the stiffness matrix as described in Procedure 1, solving the linear system and pre-computing the stresses. For all three types of elements the same code is used, except for the method to compute the derivatives. This method depends on the finite elements used and is illustrated in Procedure 2 for Catmull-Clark elements. Note that for the computations, the database was pre-computed, such that Procedure 2 for the computation of the derivatives of the hex_{CC} elements always terminates in line five.

The reference solution in Figure 8 is the black line at the normalized maximum displacement of 1. The line charts show that Catmull-Clark elements (blue lines) converge faster than other elements independently of the discretization (red and green lines). For meshes with the same number of hexahedra, the assembly is fastest for hex_8 elements and slowest for hex_{CC} elements. Solving the linear system of equations is also fastest with hex_8 elements, but hex_{CC} elements are just slightly slower. Solving the linear system of equations for hex_{20} elements takes much longer. Although this may depend on the larger number of degrees of freedoms, the overall convergence rate of hex_{20} elements compared to hex_{CC} elements is slower as well.

Figure 9 shows another example with $11,196$ hexahedra, $39,797$ edges and $14,840$ vertices. In this mesh only $1,806$ vertices and $15,645$ edges are regular. To generate this mesh we transformed a tetrahedral mesh into a hexahedral mesh by splitting each tetrahedron into four hexahedra. The characteristic of this splitting operation is that the generated mesh is highly unstructured [Owe98]. To the top of this model a vertical load is applied. The legs are fixed at the bottom. The maximum nodal displacement measured
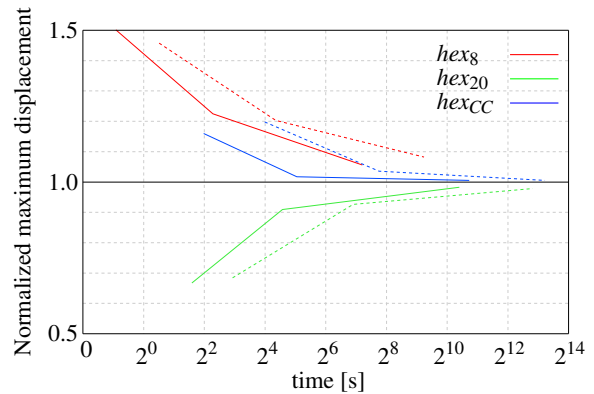
is 0.1776 mm, 0.1824 mm and 0.1811 mm for hex_8, hex_{20} and hex_{CC} elements, respectively. It shows that our algorithm also works for highly unstructured meshes.
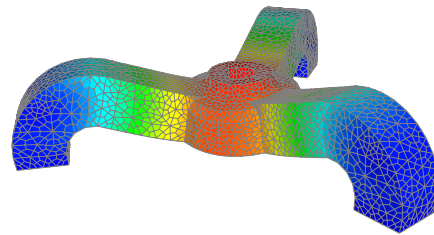

Figure 9: *Visualization of displacement field of an highly unstructured hexahedral mesh. For the visualization the same color scale is used as before.*

However, the evaluation of regular structured grids is much faster, because for regular elements basis functions can be directly applied. For irregular elements, we have to compute subdivision stencils for each sampling point in a preprocessing step and during the assembly the corresponding stencils are looked up in a database before they are applied. Therefore, we recommend to use meshes that are as regular as possible. Such a model is shown in Figure 10. This mesh has some irregular vertices, but most parts of the mesh are regular. However, in the base mesh and after one subdivision level (column one and two) all hexahedra are irregular as they lie on the boundary. In the third subdivision level about the half of the elements are regular.

9. Conclusions and future research

We have presented an iso-geometric approach for finite element analysis based on Catmull-Clark solids. The major advantage of this approach is that only one representation is re-
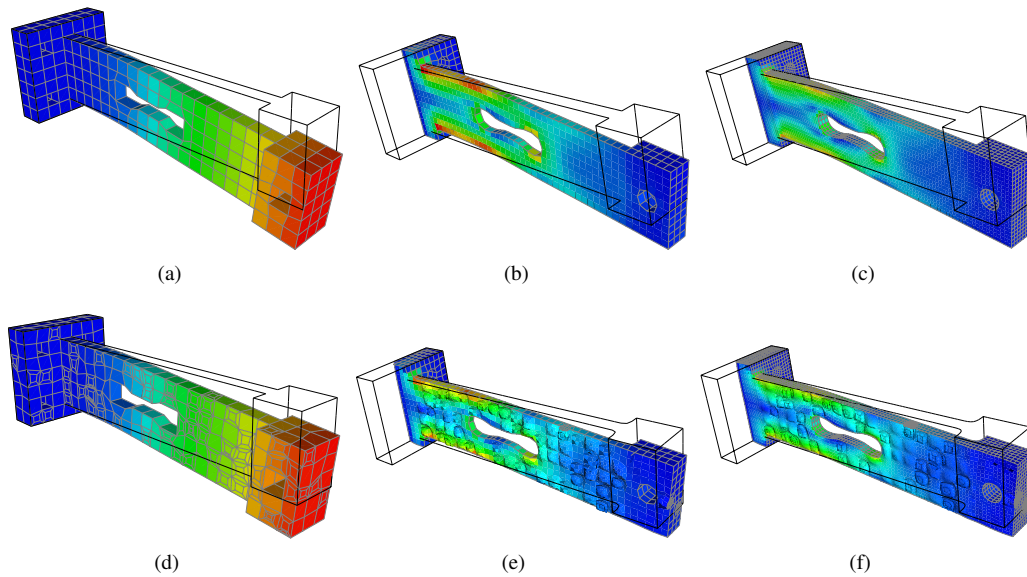
Figure 7: *Model of a load cell used for analyzing the convergence of our approach and to compare it to standard finite elements. a) regular structured mesh, d) irregular structured mesh; b) and e) meshes refined once; c) and f) meshes refined twice; a) and d) visualize the displacement field; b),c),e) and f) visualize the highest principal stress per element.*

quired for geometric design and physical analysis to narrow the gap between CAD and CAE. This is the first approach for iso-geometric finite element analysis that supports both, unstructured grids and solids. Although Catmull-Clark elements have cubic degree, the same topological mesh structure as for standard tri-linear hexahedral elements can be used. However, Catmull-Clark elements exhibit faster convergence than the standard finite element approach.

At the moment only hexahedral meshes are supported but we are working on ideas how to generalize this approach to arbitrary polyhedral meshes. Furthermore, we have illustrated this approach only for examples using linear static elasticity problems. We plan to apply our technique to other physical problems, e.g. dynamic non-linear elasticity problems and problems from fluid dynamics.

10. Acknowledgments

References

[BCC*10] BAZILEVS Y., CALO V., COTTRELL J., EVANS J., HUGHES T., LIPTON S., SCOTT M., SEDERBERG T.: Iso-geometric analysis using T-splines. *Comp. Meth. in Applied Mech. and Eng. 199*, 5-8 (2010), 229 – 263. 1, 2

[BLZ00] BIERMANN H., LEVIN A., ZORIN D.: Piecewise smooth subdivision surfaces with normal control. In *SIGGRAPH* (2000), pp. 113–120. 3

[BMZB02] BIERMANN H., MARTIN I. M., ZORIN D., BERNARDINI F.: Sharp features on multiresolution subdivision surfaces. *Graph. Models 64*, 2 (2002), 61–77. 3

[BN96] BRO-NIELSEN M.: Surgery simulation using fast finite elements. In *Proc. 4th Int. Conf. on Vis. in Biomed. Comp.* (1996), pp. 529–534. 1

[BSWX02] BAJAJ C., SCHAEFER S., WARREN J., XU G.: A subdivision scheme for hexahedral meshes. *The Visual Computer 18* (2002), 343–356. 3, 4

[CC78] CATMULL E., CLARK J.: Recursively generated B-spline surfaces on arbitrary topological meshes. *Computer-Aided Design 10*, 6 (1978), 350–355. 3

[CMQ02] CHANG Y.-S., MCDONNELL K. T., QIN H.: A new solid subdivision scheme based on box splines. In *Proc. 7th ACM Symp. on Solid Modeling and Appl.* (2002), pp. 226–233. 3

[CMQ03] CHANG Y.-S., MCDONNELL K. T., QIN H.: An interpolatory subdivision for volumetric models over simplicial complexes. In *Proc. Shape Modeling Intl.* (2003), pp. 143–152. 3

[COS00] CIRAK F., ORTIZ M., SCHRÖDER P.: Subdivision surfaces: A new paradigm for thin-shell finite-element analysis. *Int. J. Num. Meth. Eng. 47* (2000), 2039–2072. 2

[CSA*02] CIRAK F., SCOTT M. J., ANTONSSON E. K., ORTIZ M., SCHRÖDER P.: ntegrated modeling, finite-element analysis, and engineering design for thin-shell structures using subdivision. *Computer-Aided Design 34* (2002), 137–148. 2

[DEG*99] DEMMEL J., EISENSTAT S., GILBERT J., LI X., LIU J.: A supernodal approach to sparse partial pivoting. *SIAM J. Matrix Ana. and Appl. 20*, 3 (1999), 720–755. 8

[DKT98] DEROSE T., KASS M., TRUONG T.: Subdivision surfaces in character animation. *SIGGRAPH* (1998), 85–94. 3

[DLG90] DYN N., LEVINE D., GREGORY J. A.: A butterfly subdivision scheme for surface interpolation with tension control. *ACM Trans. Graph. 9*, 2 (1990), 160–169. 3
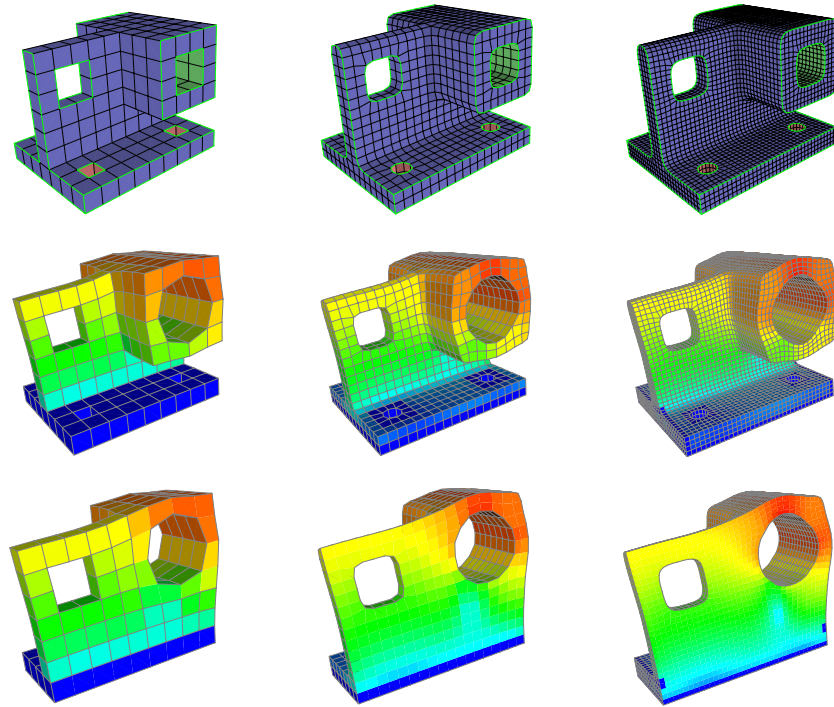
Figure 10: *Simulation of a mechanical part for three levels of refinement. First row: undeformed mesh, second row: deformation field, third row: cut-away showing stress field in the interior. First column: base mesh, second column: one-time refined mesh, third column: two-times refined mesh. This model is fixed at the drill holes at the bottom (highlighted in red) and a radial force is applied to the green highlighted faces of the models shown in the first row.*

[DS78] DOO D., SABIN M.: Behaviour of recursive division surfaces near extraordinary points. *Computer-Aided Design 10*, 6 (1978), 356–360. 3

[GJ90] GAREY M. R., JOHNSON D. S.: *Computers and Intractability; A Guide to the Theory of NP-Completeness.* W. H. Freeman & Co., 1990. 7

[HCB05] HUGHES T. J. R., COTTRELL J. A., BAZILEVS Y.: Isogeometric analysis: CAD, finite elements, NURBS, exact geometry and mesh refinement. *Comp. Meth. in Applied Mech. and Eng. 194*, 39-41 (2005), 4135–4195. 2

[ISF07] IRVING G., SCHROEDER C., FEDKIW R.: Volume conserving finite element simulations of deformable models. In *SIGGRAPH* (2007), p. 13. 1

[JM96] JOY K., MACCRACKEN R.: *The refinement rules for Catmull-Clark solids.* Tech. Rep. 96-1, UC Davis, 1996. 3, 4

[KFBY99] KAGAN P., FISCHER A., BAR-YOSEPH P. Z.: Integrated mechanically based cae system. In *ACM Symposium on Solid modeling and applications* (1999), pp. 23–30. 2

[Kob00] KOBBELT L.: $\sqrt{3}$ subdivision. In *SIGGRAPH* (2000), pp. 103–112. 3

[Loo87] LOOP C.: *Smooth Subdivision Surfaces Based on Triangles.* Master's thesis, University of Utah, 1987. 3

[Mer09] MERGHEIM J.: A variational multiscale method to model crack propagation at finite strains. *Int. J. Num. Meth. Eng. 3* (2009), 269–289. 1

[MJ96] MACCRACKEN R., JOY K.: Free-form deformations with lattices of arbitrary topology. In *SIGGRAPH* (1996), pp. 181–188. 3

[Owe98] OWEN S. J.: A survey of unstructured mesh generation technology. In *International Meshing Roundtable* (1998), pp. 239–267. 8

[Pas02] PASCUCCI V.: Slow growing volumetric subdivision. In *SIGGRAPH* (2002), pp. 251–251. 3

[PR08] PETERS J., REIF U.: *Subdivision Surfaces.* Springer, 2008. 3

[PTVF07] PRESS W. H., TEUKOLSKY S. A., VETTERLING W. T., FLANNERY B. P.: *Numerical Recipes: The Art of Scientific Computing.* Cambridge University Press, 2007. 4

[SG04] SMITH I., GRIFFITHS D.: *Programming the Finite Element Method.* Wiley, 2004. 4, 5, 6

[SHW04] SCHAEFER S., HAKENBERG J., WARREN J.: Smooth subdivision of tetrahedral meshes. In *Symp. on Geometry Processing* (2004), pp. 147–154. 3

[Sta98] STAM J.: Exact evaluation of Catmull-Clark subdivision surfaces at arbitrary parameter values. In *SIGGRAPH* (1998). 6

[Sta99] STAM J.: Evaluation of Loop subdivision surfaces. *SIGGRAPH* (1999). 6

[ZT00] ZIENKIEWICZ O., TAYLOR R.: *The Finite Element Method, Volume 1+2*, 5th ed. Butterworth, 2000. 5